

Anyonic self-induced disorder in a stabilizer code: quasi-many body localization in a translational invariant model

H. Yarloo,¹ A. Langari,^{1,2,*} and A. Vaezi³

¹*Department of Physics, Sharif University of Technology, P.O.Box 11155-9161, Tehran, Iran*

²*Center of excellence in Complex Systems and Condensed Matter (CSCM),
Sharif University of Technology, Tehran 14588-89694, Iran*

³*Department of Physics, Stanford University, Stanford, CA 94305, USA*

We enquire into the quasi-many-body localization in topologically ordered states of matter, revolving around the case of Kitaev toric code on ladder geometry, where different types of anyonic defects carry different masses induced by environmental errors. Our study verifies that random arrangement of anyons generates a complex energy landscape solely through braiding statistics, which suffices to suppress the diffusion of defects in such multi-component anyonic liquid. This non-ergodic dynamic suggests a promising scenario for investigation of quasi-many-body localization. Computing standard diagnostics evidences that, in such disorder-free many-body system, a typical initial inhomogeneity of anyons gives birth to a glassy dynamics with an exponentially diverging time scale of the full relaxation. A by-product of this dynamical effect is manifested by the slow growth of entanglement entropy, with characteristic time scales bearing resemblance to those of inhomogeneity relaxation. This setting provides a new platform which paves the way toward impeding logical errors by self-localization of anyons in a generic, high energy state, originated in their exotic statistics.

PACS numbers: 75.10.Jm, 03.75.Kk, 05.70.Ln, 72.15.Rn

Many-body localization (MBL) [1–6] generalizes the concept of single particle localization [7] to isolated interacting systems, where many-body eigenstates in the presence of sufficiently strong disorder can be localized in a region of Hilbert space, even at non-zero temperature. An MBL system comes along with universal characteristic properties, such as area-law entanglement of highly excited states (HES) [5, 8], power-law decay and revival of local observables [9, 10], logarithmic growth of entanglement after a global quench [11–14] as well as the violation of “eigenstates thermalization hypothesis” (ETH) [15–17]. The latter raises the appealing prospect of protecting quantum order, storage and manipulating coherent information in the out-of-equilibrium many-body states [18–22].

Recently, it has been realized [23–32] that quench disorder is not essential to induce localization and ergodicity breaking could emerge solely from interactions in translationally-invariant systems. Almost all previous studies are restricted to models involving either admixture of strongly interacting particles, i.e. heavy and light particles, or single species models with long-range interactions. In such systems, initial random arrangement of particles, effectively induces strong tendency toward self-localization, which is characterized by MBL-like behavior of the growth of entanglement entropy, tagged quasi-many-body localization (qMBL), and dynamical persistence of a typical initial inhomogeneity. However, this non-ergodic behavior, in contrast to the standard scenario of MBL, is not necessarily accompanied by the emergence of the infinite number of conserved quantities [33–36].

Here, we introduce a novel mechanism toward qMBL

in a family of translationally invariant quantum double models, in particular Kitaev toric code [37, 38] on ladder geometry [39, 40], a.k.a. Kitaev ladder (KL). The elementary excitations of KL system are associated with point-like quasiparticles, known as charge and flux anyons. Our main interest in this model has its roots in the role of non-trivial statistics between anyons that naturally live in (highly) excited states of KL.

Anyons are potentially promising candidates for fault-tolerant quantum computation, which received growing attentions [37, 38, 41, 42]. In particular, *non-Abelian* anyons obtain a classical diffusive behavior due to their structural entanglement [43, 44], having a well built tendency toward thermalization [45] even in a strongly disordered environment [46]. On the other hand, for *Abelian* anyons the situation differs: introducing disorder in an Abelian stabilizer code ensures the single particle localization of anyons living in low-lying excited states [47, 48]. The main inquiries which have emerged from these studies are whether it is possible to localize anyons in HES of such topologically ordered systems by means of qMBL mechanism, and besides, what is the advantage of this type of localization with respect to disorder-dominated one in topological quantum memories?

We address this questions by showing that random configurations of Abelian anyons in HES of KL can induce a self-generated disorder, purely due to braiding statistics between anyons. By performing a dual mapping we show that, the presence of non-zero density of static fluxes, as barriers, can put kinetic constraint on dynamic of charges as light particles. This effect traps charges between flux barriers and hinders the propagation of them on non-

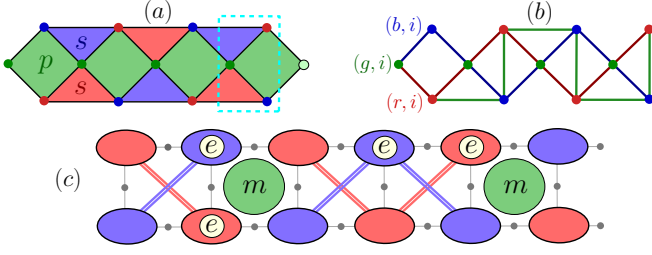


FIG. 1. (a) KL model with periodic-boundary condition (periodic-BC) in leg (x-direction) and open-BC along rungs (y-direction). Spin-1/2 particles are placed on the $3L$ nodes of the lattice. (b) Multiplying Z operators along the red (blue) line yields dual spin $\mu_{r/b,i}^x$, and a similar string of X operators along the green line defines $\mu_{g,i}^x$. (c) The pictorial demonstration of the dual KL model, Eq. (4), for $t_m = 0$.

trivial class of loops around the cylindrical surface of KL. Additionally, we find that the presence of flux favors the robustness of SPT phase by obstructing the perturbation effects. Finally, we provide numerical evidences, obtained by exact diagonalization, that the effective disorder leads to the existence of an exponentially diverging time scale for dynamical persistence of initial inhomogeneity, along with the growth of entanglement entropy that displays slow MBL-like behavior in the intermediate time, all of which are essential qualities of qMBL. Furthermore, we compute ETH indicators for testing thermalization of local observables, in agreement with the mentioned behaviors.

Kitaev ladder Hamiltonian.— The Kitaev ladder (KL) is defined on a quasi-1D ladder with L unit cells, each one with three sites, that we will refer to as red, green, and blue sites (see Fig. 1-(a)). The unperturbed Hamiltonian is composed of L plaquette stabilizer, B_p , and $2L$ vertex stabilizer terms on the triangles on the ladder, $A_s^{r/b}$, as follows:

$$H_0^{KL} = -j_m \sum_i B_p(i) - j_e \sum_i (A_s^r(i) + A_s^b(i)), \quad (1)$$

$$(2)$$

$$B_p(i) = Z_{g,i} Z_{r,i} Z_{b,i} Z_{g,i+1},$$

$$A_s^{r/b}(i) = X_{r/b,i-1} X_{g,i} X_{b/r,i},$$

where X_i and Z_i are the x- and z-component of Pauli operators, respectively. We set $j_e, j_m > 0$ and choose an overall energy scale by setting $j_e = 1$. The KL model can be viewed as the Kitaev toric code (KTC) with surface termination along the y direction (a.k.a. surface code) whose width is one. Thus, it is easy to verify that it inherits the topological order of the KTC [49]. Now we would like to perturb the KL such that the electric (e) and magnetic (m) charges, corresponding to $A_s = -1$ and $B_p = -1$, respectively, can hop across the ladder and gain kinetic energy. This can be achieved, for instance, for an e charge on site (r, i) via applying $Z_{g,i} Z_{r,i}$ operator,

which commutes with every plaquette and star operator except $A_s^r(i)$ and $A_s^r(i+1)$ and thus transfers the e charge to $(r, i+1)$. We could also use $Z_{b,i} Z_{g,i+1}$ to carry out the same task, where symmetry considerations dictate the two terms must have identical amplitudes. However, $Z_{b,i} Z_{g,i+1} = B_p(i) Z_{g,i} Z_{r,i}$, and therefore the total contribution to the Hamiltonian is $(1 + B_p(i)) Z_{g,i} Z_{r,i}$. As one can see, the Ising interactions are coupled to a dynamical \mathbb{Z}_2 gauge field and thus hopping of an e charge from (r, i) to $(r, i+1)$ depends on the value of $B_p(i) = (-1)^{n_m(i)}$, which takes into account the parity of m anyon on site (g, i) , or equivalently, the mutual braiding statistics of e and m . Hence, the hopping of e is blocked if there is a flux on its way. Here, $n_m(i)$ is either 0 or 1, corresponding to the absence or presence of a flux at plaquette i .

Likewise, $X_{r,i} X_{b,i+1}$ transports one unit of flux (m) from site (g, i) to $(g, i+1)$ and vice versa. We could also consider $X_{b,i} X_{r,i+1}$ to reach the same goal. However, $X_{b,i} X_{r,i+1} = A_s^r(i+1) A_s^b(i+1) X_{r,i} X_{b,i+1}$, and again the movement of m anyon is intertwined with the density of e charges along its way. Therefore, we study the following perturbed KL model:

$$H^{KL} = H_0^{KL} - t_e \sum_i (Z_{g,i} Z_{r,i} + Z_{g,i} Z_{b,i}) (1 + B_p(i))$$

$$- t_m \sum_i X_{r,i} X_{b,i+1} (1 + A_s^r(i+1) A_s^b(i+1)) \quad (3)$$

where t_e (t_m) is the hopping strength of electric (magnetic) charges.

It is worth mentioning that we can use a duality transformation to map the above Hamiltonian to three coupled transverse field Ising (TFI) models (see Fig. 1-(b)), after which

$$H_{\text{dual}}^{KL} = - \sum_i (j_m \mu_{g,i}^z + t_m \mu_{g,i}^x \mu_{g,i+1}^x (1 + \mu_{r,i+1}^z \mu_{b,i+1}^z))$$

$$- \sum_i (j_e \mu_{b,i}^z + t_e \mu_{b,i}^x \mu_{b,i+1}^x (1 + \mu_{g,i}^z))$$

$$- \sum_i (j_e \mu_{r,i}^z + t_e \mu_{r,i}^x \mu_{r,i+1}^x (1 + \mu_{g,i}^z)), \quad (4)$$

where

$$\mu_{g,i}^x = \prod_{j \geq i} X_{r,j} X_{b,j+1}, \quad \mu_{r/b,i}^x = \prod_{j \geq i} Z_{g,j} Z_{r/b,j},$$

and $\mu_{g,i}^z = B_p(i)$, $\mu_{r/b,i}^z = A_s^{r/b}(i)$.

Anyonic self-induced disorder in the KL.— Here, we investigate the localization effect of the perturbed KL model, Eq. (3), that takes the general form of Falicov-Kimball like Hamiltonians [24]. We first examine the $t_m = 0$ case, corresponding to static magnetic charges. Next, we consider nonzero t_m and by utilizing various diagnostics we show that in the regime where $t_m \ll t_e$, i.e. magnetic charges are heavy and electric charges are light anyons, the system is in the qMBL phase. The flux density is denoted by ρ_m and the electric charge density by $\rho_e \cdot t_e$.

A. Immobile magnetic charges ($t_m = 0$).— The model is composed of m anyons, which are immobile and cannot hop along the ladder. They form a set of L constants of motion with trivial dynamics that can be treated as classical variables, $\{B_p(i)\} = \pm 1$. The existence of a flux in each plaquette, characterized by the probability ρ_m , prompts a quench disorder, $t'_e(i) = t_e(1 + B_p(i))$, and *energetically* suppresses charge's kinetic interaction.

Therefore, the presence of fluxes—in addition to increasing the energy density by the first term of H_0^{KL} in Eq. (1)—brings on an effective *self-generated disorder* with the following dilution distribution,

$$\mathcal{P}(t'_e) = (1 - \rho_m)\delta(t'_e - 2t_e) + \rho_m\delta(t'_e), \quad (5)$$

where for a fixed value of ρ_m , different realizations of disorder correspond to different configurations of fluxes.

Apart from that, in this case the dual KL model (4) reduces to two decoupled TFI chains subject to effective random diluted exchange interaction, Eq. (5). Hence, it is evident that charge anyons are trapped in the intervals between static flux barriers with no interaction with the particles outside as well, see Fig. 1(c). Accordingly, the dynamic of charges is strongly non-ergodic, and the diffusion of them that creates logical errors will be restrained by the massive flux barriers.

In $\rho_m = 0$ sector, the system becomes even more straightforward to analyze, in which $\mu_{g,i}^z = 1$ everywhere. As a result, H_{dual}^{KL} reduces to two clean TFI chains, and from the Jordan-Wigner transformation one understands that there is a phase transition at $t_e^c = 1/2$. The $t_e < 1/2$ is smoothly connected to the $t_e = 0$ phase, where the system is unperturbed and represents a $\mathbb{Z}_2 \times \mathbb{Z}_2$ symmetry protected topological (SPT) phase [40], while $t_e > 1/2$ is smoothly connected to the $j_e = 0$ fixed point and represents the trivial polarized phase. However, as we show below, for nonzero flux density ($\rho_m > 0$) there is no phase transition and the topological order is robust against the hopping of e anyons as long as $t_m = 0$.

To reveal the effect of nonzero flux density on the robustness of SPT order, we first focus on H_{dual}^{KL} in its finite flux density sectors. According to the exact solution presented in Ref. 50, for arbitrary (increasing) values of t_e , even an infinitesimal (nonzero) ρ_m spoils any long range magnetic order in the thermodynamic limit. For this reason, in terms of pseudo-spin operators $\mu_{r/b,i}$, of the dual transformation, the two chains are always in the paramagnetic phase, which in the language of the original model is identical to the SPT phase of KL [49]. Thus, the existence of flux anyons (such that ρ_m remains finite in the limit $L \rightarrow \infty$) favors topological order in the system. However, for the low energy states in free flux sector, $\rho_m = 0$, this effect eventually diminishes and eigenstates become extended.

B. quasi-MBL phase.— We are now ready to address the following question: whether ergodicity could be restored if we consider a large but finite effective mass for

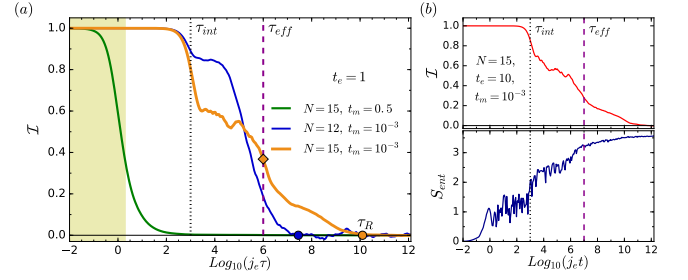


FIG. 2. (a) Relaxation of flux inhomogeneity density for $t_e = 1$ and $j_m = 10$, averaged over 150 random initial states. For $t_m = 0.5$, the fast relaxation occurs until the characteristic time τ_{int} (shaded region). The time scales τ_{int} and τ_{eff} for $t_m = 10^{-3}$ are shown by black dotted and purple dashed lines, respectively. For this case, complete relaxation occurs at τ_R , which displays exponentially diverging behavior. (b) Upper panel: Relaxation of flux inhomogeneity density for $t_e = 10$ and $j_m = 50$, averaged over 150 random initial configurations. Lower panel: Entanglement dynamics for cutting at 8-th spin, averaged over 250 random product states. The time interval in which the residual inhomogeneity at τ_{eff} vanishes match up with that of the entanglement exhibiting the final growth before complete saturation.

m anyons, i.e. $0 < t_m \ll t_e$ regime? In this case, the fluxes are mobile and can hop along the ladder and as a result, the dynamics of m and e anyons are intertwined. In this respect, after preparing the whole system in a completely localized and inhomogeneous random configuration of anyons, $|\psi_0\rangle$, which is selected near the middle of the spectrum of H^{KL} , we compute the non-equilibrium time average $\overline{\Delta N_m^2(\tau)} \equiv \frac{1}{\tau} \int_0^\tau dt \Delta N_m^2(t)$, of the average inhomogeneity of fluxes:

$$\Delta N_m^2(t) \equiv \frac{1}{L} \sum_{p=1}^L |\langle \psi_0 | (n_m(p+1; t) - n_m(p; t)) | \psi_0 \rangle|^2. \quad (6)$$

At long times, the dynamical equilibrium value of $\overline{\Delta N_m^2(\tau)}$ vanishes for any perfect delocalized state, while $\overline{\Delta N_m^2(\infty)}$ remains finite in any finite-size translationally invariant model. Hence we compute -

$$\mathcal{I}(\tau) = \frac{\overline{\Delta N_m^2(\tau)} - \overline{\Delta N_m^2(\infty)}}{\overline{\Delta N_m^2(0)} - \overline{\Delta N_m^2(\infty)}}, \quad (7)$$

which asymptotically tends to zero for $\tau \rightarrow \infty$.

$\mathcal{I}(\tau)$ is depicted in Fig. 2(a) for two values of $t_m = 0.001$ and 0.5 , corresponding to slow and fast flux dynamics, respectively. For the fast dynamics, a rapid relaxation occurs in the initial inhomogeneity due to resonance admixture within the time scale $\tau_{int} \sim t_m^{-1}$ (represented by shaded regions in Fig. 2(a)), which is the characteristic time of introducing effective interaction to the system. For $t_m = 0.001$, the initial inhomogeneity plateau persists until τ_{int} . Moreover, a significant residual inhomogeneity

exists even at later times, $\tau_{eff} \sim t_e/t_m^2$. The slow, coherent dynamics of fluxes—due to their collective motion—has a characteristic time, τ_R , in which \mathcal{I} completely relaxes. This time scale for $N = 15$ is at least 100 times longer than that of $N = 12$. Hence, we expect τ_R to grow exponentially with flux density and system size, which states that the translational symmetry is dynamically broken, stronger

To better understand the nature of these time scales, we have also looked at the growth of entanglement entropy $S_{ent} = -\rho_A \ln \rho_A$ (after the division of the system into A and B subregions), averaged over 50-250 random initial product states. As depicted in Fig. 2(b), prior to the time scale τ_{int} , charges perceive the fluxes as if they are immobile barriers that are coupled to their kinetic terms via a local \mathbb{Z}_2 gauge field. Hence, after an initial growth (until j_e^{-1}), S_{ent} saturates to the first plateau, conveying a rapid Gaussian spreading of the initial wave packet to the single particle localization length of charges. In fact, passage of time reveals the early non-interacting, disordered nature of the system. Subsequent to τ_{int} , hybridization of fluxes arrives, which introduces interaction to the charge dynamics. Thus, the entropy shows logarithmic growth until the finite-size dephasing of charge quasi-particles wins at the second plateau. Eventually, at τ_{eff} , dephasing of the flux particles sets in, and the entanglement grows even much slower to saturate at the last finite-size plateau. Crucially, the same time scales also determine the evolution of initial inhomogeneity. Recently, an identical effect has been observed in an interacting admixture of spins on ladder geometry [31]. The central disparity arises here is that in KL, there only exists one type of spin 1/2, where different elementary excitations (e and m) have no direct interaction except the interaction induced by nontrivial braiding statistics.

Lastly, we would like to address whether the self-localization in such anyonic liquid is followed by failing ETH for excited states? to this end, we discard the creation/annihilation of fluxes which might happen as a result of $X_{r,i}X_{b,i+1}$ terms in Eq. (3). Typically, this recombining processes are less likely for the heavy particles in comparison to the light ones. So, it is a reasonable assumption to consider $\tilde{H}_{KL} = \hat{P}_{N_m} H^{KL} \hat{P}_{N_m}$, for reaching larger system sizes, where \hat{P}_{N_m} is the projection operator to the subspace with total flux number N_m [49]. We evaluate $\mathcal{G} \equiv \langle n_p^m n_{p+1}^m \rangle$ in the simultaneous eigenstates of \tilde{H}_{KL} and momentum (hence we only consider \mathcal{G} for $p = 1$) and collect the results from all momenta. Working with the momentum basis—which have perfect homogeneity—disentangles the effect of glassy dynamics on failing of thermalization in our model. We report the results for different system sizes and total flux numbers $(N, N_m) = (12, 2)$, $(15, 3)$ and $(18, 3)$ within two different cases $(t_e, t_m) = (1, 0.001)$ and $(1, 0.5)$, correspond-

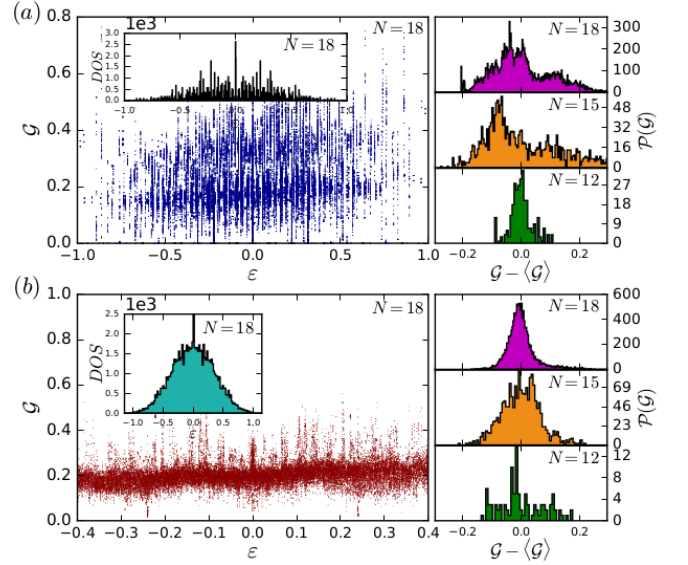


FIG. 3. (a) Failing of ETH for the case $(t_e, t_m) = (1, 0.001)$. Left panel: The expectation value \mathcal{G} in momentum eigenstates versus energy density. Inset shows DOS for the Hamiltonian \tilde{H}_{KL} , which split to numerous mini bands. Right panel: distribution of the value \mathcal{G} ($\mathcal{P}(\mathcal{G})$) for all eigenstates in the energy window $\epsilon \in [-0.09, 0.09]$ in the middle of the energy band for different system sizes. The average value is removed from the distribution for visibility. (b) Validity of ETH for the case $(t_e, t_m) = (1, 0.5)$ corresponding to fast relaxation dynamics. Here, $\mathcal{P}(\mathcal{G})$ is plotted for the eigenstates in $\epsilon \in (0, 0.15]$.

ing to the slow and fast relaxation dynamics, respectively.

We plot \mathcal{G} versus energy density, $\epsilon = E/N$, for $(t_e, t_m) = (1, 0.001)$ in Fig. 3-(a). In the whole energy intervals the value of \mathcal{G} is spread considerably in a wide range and the density of states (DOS) consists of numerous mini-bands. Besides that, the distribution of \mathcal{G} , $\mathcal{P}(\mathcal{G})$, near the middle of the band, where $\epsilon \in [-0.09, +0.09]$, has a very broad half-width and peaks at different values as the system size is increased (right panel in Fig. 3-(a)), which provides strong non-ergodic behavior.

For the fast dynamical relaxation, $(t_e, t_m) = (1, 0.5)$, the system rather obeys ETH prediction: DOS becomes continuous, $\mathcal{P}(\mathcal{G})$ sharply picks around its mean value and the width of distribution decreases by increasing system size, as illustrated in Fig. 3-(b). Hence, by increasing t_m the model encounters a phase transition from a qMBL phase to an ETH one.

Discussion.—We showed that in high energy configurations of a topologically ordered stabilizer system, random arrangement of anyons produces a complex energy landscape, which energetically suppresses anyonic diffusion via qMBL mechanism. As we argued, the self-induced localization stems from the entanglement structure based on the nontrivial mutual statistics. This is a novel mechanism and distinct from the previous studies

on qMBL [24, 27, 31, 32, 51].

A profitable feature of qMBL (with the underlying mechanism), in comparison to standard MBL, is the reversed role of temperature and interaction. Within our framework, this fact embodies itself in the following statements: the stronger environmental perturbations, the higher strength of self-disorder. Moreover, moving to higher energy density leads to more configurational disorder, all of which boosting the tendency of anyons toward self-localization.

Our work suggests that the nontrivial braiding statistics of anyons could enhance the memory lifetime by generating glassy dynamics within the system. The scenario discussed in this work can be easily generalized [49] to other quantum double models such as Levin-Wen model [52].

A closely related concept to qMBL in multi-component systems is quantum disentangled liquid (QDL) [51, 53, 54], wherein partial thermalization occurs as a result of “post-measurement” process, identical to error syndrome measurement in our model. It is tempting to see whether such measurement procedure on a topological state supports this claim. Intuitively, could there a quantum disentangled *spin* liquid (QDSL) phase be found?

Acknowledgment.—We highly appreciate fruitful discussions and neat comments by M. Najafi Ivaki and M. Mohseni Rajaei. The authors would like to thank Sharif University of Technology for financial supports. AV was supported by Gordon and Betty Moore foundation.

* langari@sharif.edu

- [1] I. V. Gornyi, A. D. Mirlin, and D. G. Polyakov, *Phys. Rev. Lett.* **95**, 206603 (2005).
- [2] Basko D.M., Aleiner I.L., and Altshuler B.L., *Annals of Physics* **321**, 11261205 (2006).
- [3] V. Oganesyan and D. A. Huse, *Phys. Rev. B* **75**, 155111 (2007).
- [4] A. Pal and D. A. Huse, *Phys. Rev. B* **82**, 174411 (2010).
- [5] B. Bauer and C. Nayak, *Journal of Statistical Mechanics: Theory and Experiment* **2013**, P09005 (2013).
- [6] J. Z. Imbrie, *Journal of Statistical Physics* **163**, 9981048 (2016).
- [7] P. W. Anderson, *Phys. Rev.* **109**, 1492 (1958).
- [8] J. A. Kjäll, J. H. Bardarson, and F. Pollmann, *Phys. Rev. Lett.* **113**, 107204 (2014).
- [9] M. Serbyn, Z. Papić, and D. A. Abanin, *Phys. Rev. B* **90**, 174302 (2014).
- [10] M. Serbyn, M. Knap, S. Gopalakrishnan, Z. Papić, N. Y. Yao, C. R. Laumann, D. A. Abanin, M. D. Lukin, and E. A. Demler, *Phys. Rev. Lett.* **113**, 147204 (2014).
- [11] M. Žnidarič, T. c. v. Prosen, and P. Prelovšek, *Phys. Rev. B* **77**, 064426 (2008).
- [12] J. H. Bardarson, F. Pollmann, and J. E. Moore, *Phys. Rev. Lett.* **109**, 017202 (2012).
- [13] R. Vosk and E. Altman, *Phys. Rev. Lett.* **110**, 067204 (2013).
- [14] M. Serbyn, Z. Papić, and D. A. Abanin, *Phys. Rev. Lett.* **110**, 260601 (2013).
- [15] J. M. Deutsch, *Phys. Rev. A* **43**, 2046 (1991).
- [16] M. Srednicki, *Phys. Rev. E* **50**, 888 (1994).
- [17] M. Rigol, V. Dunjko, and M. Olshanii, *Nature* **452**, 854858 (2008), 10.1038/nature06838.
- [18] D. A. Huse, R. Nandkishore, V. Oganesyan, A. Pal, and S. L. Sondhi, *Phys. Rev. B* **88**, 014206 (2013).
- [19] A. Chandran, V. Khemani, C. R. Laumann, and S. L. Sondhi, *Phys. Rev. B* **89**, 144201 (2014).
- [20] Bahri Yasaman, Vosk Ronen, Altman Ehud, and Vishwanath Ashvin, *Nature Communications* **6**, 7341 (2015).
- [21] A. C. Potter and A. Vishwanath, ArXiv e-prints (2015), arXiv:1506.00592 [cond-mat.dis-nn].
- [22] N. Y. Yao, C. R. Laumann, and A. Vishwanath, ArXiv e-prints (2015), arXiv:1508.06995 [quant-ph].
- [23] S. M. F. M. Carleo G, Becca F, *Scientific Reports* **2**, 243 (2011).
- [24] M. Schiulaz and M. Müller, *AIP Conference Proceedings* **1610**, 11 (2014).
- [25] W. De Roeck and F. Huveneers, *Communications in Mathematical Physics* **332**, 10171082 (2014).
- [26] W. De Roeck and F. m. c. Huveneers, *Phys. Rev. B* **90**, 165137 (2014).
- [27] M. Schiulaz, A. Silva, and M. Müller, *Phys. Rev. B* **91**, 184202 (2015).
- [28] Z. Papić, E. M. Stoudenmire, and D. A. Abanin, *Annals of Physics* **362**, 714 (2015).
- [29] L. Barbiero, C. Menotti, A. Recati, and L. Santos, *Phys. Rev. B* **92**, 180406 (2015).
- [30] J. M. Hickey, S. Genway, and J. P. Garrahan, *Journal of Statistical Mechanics: Theory and Experiment* **2016**, 054047 (2016).
- [31] N. Y. Yao, C. R. Laumann, J. I. Cirac, M. D. Lukin, and J. E. Moore, *Phys. Rev. Lett.* **117**, 240601 (2016).
- [32] A. Smith, J. Knolle, D. L. Kovrizhin, and R. Moessner, ArXiv e-prints (2017), arXiv:1701.04748 [cond-mat.str-el].
- [33] M. Serbyn, Z. Papić, and D. A. Abanin, *Phys. Rev. Lett.* **111**, 127201 (2013).
- [34] D. A. Huse, R. Nandkishore, and V. Oganesyan, *Phys. Rev. B* **90**, 174202 (2014).
- [35] A. Chandran, I. H. Kim, G. Vidal, and D. A. Abanin, *Phys. Rev. B* **91**, 085425 (2015).
- [36] Ros V., Müller M., and Scardicchio A., *Nuclear Physics B* **891**, 420465 (2015).
- [37] E. Dennis, A. Kitaev, A. Landahl, and J. Preskill, *Journal of Mathematical Physics* **43**, 4452 (2002).
- [38] A. Kitaev, *Annals of Physics* **303**, 2 (2003).
- [39] V. Karimipour, *Phys. Rev. B* **79**, 214435 (2009).
- [40] A. Langari, A. Mohammad-Aghaei, and R. Haghshenas, *Phys. Rev. B* **91**, 024415 (2015).
- [41] D. Bacon, *Phys. Rev. A* **73**, 012340 (2006).
- [42] B. Yoshida, *Annals of Physics* **326**, 25662633 (2011).
- [43] L. Lehman, V. Zatloukal, G. K. Brennen, J. K. Pachos, and Z. Wang, *Phys. Rev. Lett.* **106**, 230404 (2011).
- [44] V. Zatloukal, L. Lehman, S. Singh, J. K. Pachos, and G. K. Brennen, *Phys. Rev. B* **90**, 134201 (2014).
- [45] A. Chandran, M. D. Schulz, and F. J. Burnell, *Phys. Rev. B* **94**, 235122 (2016).
- [46] A. C. Potter and R. Vasseur, *Phys. Rev. B* **94**, 224206 (2016).
- [47] J. R. Wootton and J. K. Pachos, *Phys. Rev. Lett.* **107**, 030503 (2011).

- [48] C. Stark, L. Pollet, A. m. c. Imamoğlu, and R. Renner, [Phys. Rev. Lett. **107**, 030504 \(2011\)](#).
- [49] See Supplementary material.
- [50] R. B. Stinchcombe, [Journal of Physics C: Solid State Physics **14**, L263 \(1981\)](#).
- [51] T. Grover and M. P. A. Fisher, [Journal of Statistical Mechanics: Theory and Experiment **2014**, P10010 \(2014\)](#).
- [52] M. A. Levin and X.-G. Wen, [Phys. Rev. B **71**, 045110 \(2005\)](#).
- [53] J. R. Garrison, R. V. Mishmash, and M. P. A. Fisher, [Phys. Rev. B **95**, 054204 \(2017\)](#).
- [54] T. Veness, F. H. L. Essler, and M. P. A. Fisher, ArXiv e-prints (2016), [arXiv:1611.02075 \[cond-mat.stat-mech\]](#).

Supplemental Material for EPAPS
Anyonic self-induced disorder in a stabilizer code:
quasi-many body localization in a translational invariant model

H. Yarloo,¹ A. Langari,^{1,2,*} and A. Vaezi³

¹*Department of Physics, Sharif University of Technology, P.O.Box 11155-9161, Tehran, Iran*

²*Center of excellence in Complex Systems and Condensed Matter (CSCM), Sharif University of Technology, Tehran 14588-89694, Iran*

³*Department of Physics, Stanford University, Stanford, CA 94305, USA*

Kitaev Ladder (KL).—We first briefly discuss the main properties of the KL Hamiltonian, H_0^{KL} , in (highly) excited states to give an insight on its nature as an anyonic liquid.

In KL periodic-boundary condition in the leg direction leads to the global constraint $\prod_i A_s^{r/b}(i) = \mathbb{1}$, which ensures that (i) any energy level in the whole spectrum will have at least twofold degeneracy and (ii) $2L-1$ independent charge degrees of freedom are created/annihilated in pairs. However, fluxes can be created/annihilated singly in contrast to the 2D toric code on torus. One can also define the occupation operators of charges and fluxes, $\hat{n}_i^e = (1 - A_s^{r/b}(i))/2$ and $\hat{n}_i^m = (1 - B_p(i))/2$, respectively. In term of occupation operators, H_0^{KL} simply counts the total number of e and m anyons in the system. The basis which diagonalizes H_0^{KL} has the following closed form in the occupation number representation:

$$|\{n_i^m\}, \{r_i\}\rangle = \hat{P}_{\{n_i^m\}} \hat{g}_{\{r_i\}} |x+\rangle^{\otimes N}, \quad (1)$$

where $\hat{P}_{\{n_i^m\}} = \prod_i (1 + (-1)^{n_i^m} B_p(i))/2$, $\hat{g}_{\{r_i\}} = \prod_{i \in D} Z_i^{r_i}$ and $|x+\rangle$ is the eigenstate of X , i.e. $X|x+\rangle = |x+\rangle$. $\hat{g}_{\{r_i\}}$ is a member of the Abelian group G (consisting of 2^{2L} different set of configurations, $\{r_i = 0, 1\}$), which performs all spin-flip operations for $2L$ spins placed on the global path D (see Fig. 1). By the action of G on the charge vacuum state, one can generate all 2^{2L-1} different independent charge configurations. $\hat{P}_{\{n_i^m\}}$ is the projection operator onto the subspace with flux configuration, $\{n_i^m\}$, where 2^L different set of $\{n_i^m = 0, 1\}$ can generate corresponding flux degrees of freedom. However, $\{r_i = 1; \forall i\}$ is a special case for which $W_z \equiv \hat{g}_{\{r_i=1\}}$ goes over the whole system on homologically nontrivial path D . Accordingly, for any state $|\{n_i^m\}, \{r_i\}\rangle$, there is a degenerate state,

$$|\{n_i^m\}, \{\bar{r}_i\}\rangle = W_z |\{n_i^m\}, \{r_i\}\rangle, \quad W_z = \prod_{i \in D} Z_i, \quad (2)$$

where W_z plays the role of *Wilson loop*, which creates a pair of charges on a vertex, rounds them across the system, and then annihilates them. This process is accompanied by changing topological sector of states and can be interpreted as diffusion of unchecked errors across the ladder after a time proportional to the system size, a.k.a. logical error. Hence, generating glassy dynamics in highly-excited states (HES) of such disorder-free stabilizer codes impedes the mentioned procedure and puts forward a new paradigm for realizing more stable quantum memories at finite temperature, the task which assigned to the quasi many-body localization (qMBL) mechanism through this work.

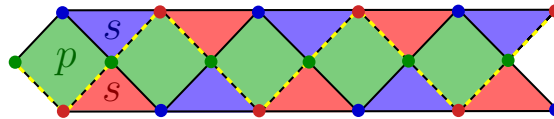


FIG. 1. KL as a surface code terminated in one direction. Dashed line indicates topologically nontrivial path D .

Furthermore, as mentioned in the main text, the ground state of KL model (with twofold degeneracy in the free charge and flux sectors $\{n_i^m = 0, r_i = 0; \forall i\}$) can not be smoothly connected to a short range entangled state without breaking the following Ising symmetries, explicitly or spontaneously:

$$\Sigma^{IZZ} = \prod_{i=1}^L B_p(i), \quad \Sigma^{XXX} = \prod_s A_s^r(i) = \prod_s A_s^b(i). \quad (3)$$

The action of these symmetries on occupation number basis Eq. (1) can be interpreted as anyonic parity, such that Σ^{IZZ} shows the *flux parity* and Σ^{XXX} represents the *charge parity* in the red or blue vertices.

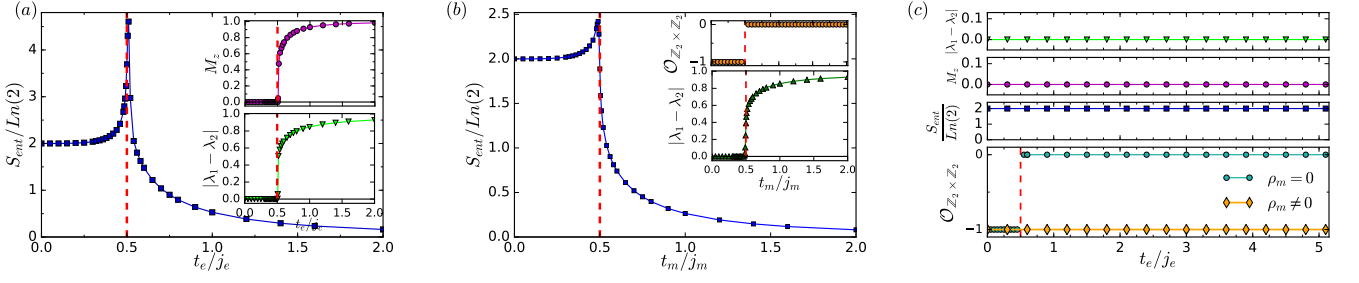


FIG. 2. (a) von-Neumann entropy (S_{ent}) calculated by an implementation of iTEBD method with $\chi = 64$ for the Hamiltonian $H^{KL}(t_m = 0)$ in $\rho_m = 0$ sector. The upper and bottom insets show magnetization (M_z) and the gap between two largest Schmidt coefficients ($|\lambda_1 - \lambda_2|$), respectively. All data shows diverging behavior at $t_e^c/j_e = 1/2$. (b) von-Neumann entropy computed for the Hamiltonian $H^{KL}(t_e = 0)$ in $\rho_e = 0$ sector. The upper and bottom insets show $\mathcal{O}_{Z_2 \times Z_2}$ defined in Eq. (4) and gap between two largest Schmidt coefficients, respectively. (c) The three top panels display the effect of nonzero density of fluxes on the same quantities plotted in (a). The lowest panel specifies the phase factor order parameter, $\mathcal{O}_{Z_2 \times Z_2}$, which reveals robustness of the SPT order for $\rho_m \neq 0$.

Robustness of SPT phase in finite flux density: Numerical approach.—Here, we would like to numerically check the validity of our analytical result, extracted from explicit dual transformation given in the main text, on topological nature of the perturbed KL, H^{KL} . In this respect, we employed infinite time-evolving block decimation (iTEBD) algorithm [1], which is based on infinite matrix-product state (iMPS) representation.

Consider the transitionally invariant H^{KL} for the case of immobile magnetic charges, $t_m = 0$, in $\rho_m = 0$ sector. We compute the half-cut von-Neumann entanglement entropy, $S_{ent} = -\text{tr}(\rho_{L/2} \ln \rho_{L/2})$, where ρ is the ground state density matrix. The main plot of Fig. 2-(a) shows a diverging behavior of S_{ent} at $t_e^c = 1/2$ (in the unit $j_e = 1$), which is a signature of quantum phase transition. Moreover, the magnetization $M_z = (\sum_i Z_i)/(3L)$ presented in the upper inset of Fig. 2-(a) shows a transition from a non-magnetic phase for $t_e < 1/2$ to a spontaneously symmetry breaking phase for $t_e > 1/2$. The lower inset of Fig. 2-(a) unveils the difference between the two largest magnitudes of Schmidt coefficients, $|\lambda_1 - \lambda_2|$, where the degeneracy of λ_1 and λ_2 for $t_e < 1/2$ is the characteristic feature of symmetry-protected topological (SPT) phase [2]. A similar behavior holds in the case $H^{KL}(t_e = 0)$ in the $\rho_e = 0$ sector, where the phase transition occurs at $(t_m^c/j_m) = 1/2$ (see Fig 2-(b)). Additionally, we computed the phase factor order parameter [3]:

$$\mathcal{O}_{Z_2 \times Z_2} = \begin{cases} 0 & \text{if } |\eta_z| < 1 \text{ or } |\eta_x| < 1 \\ \frac{1}{\chi} \text{tr}(U_z U_x U_z^\dagger U_x^\dagger) & \text{if } |\eta_z| = 1 = |\eta_x|, \end{cases} \quad (4)$$

where η_z and η_x are the largest eigenvalues of the *generalized transfer matrix* [3] constructed by symmetry operators Σ^{IZZ} and Σ^{XXX} , respectively, and U_z^\dagger and U_x^\dagger are eigenvectors corresponding to them (here χ is the bond dimension of iMPS). The symmetry protected nontrivial phase, symmetry-breaking phase and symmetry protected trivial phase are characterized by $\mathcal{O}_{Z_2 \times Z_2} = \{-1, 0, 1\}$, respectively. The behavior of all mentioned quantities implies that for $t_e < 1/2$ ($t_m < 1/2$), the perturbed system at zero flux sector (zero charge sector) belongs to the $\mathbb{Z}_2 \times \mathbb{Z}_2$ quantum spin liquid phase.

Now, we consider the parent Hamiltonian $H_0'^{KL}$, which is different from H_0^{KL} in that, we have set $j_m \rightarrow j_m' = -j_m$. The ground state of $H_0'^{KL}$ is in the full flux sector, $\rho_m = 1$, equivalent to the highest energy sector of H_0^{KL} . It can be shown that after adding the plaquette-Ising interaction (as charge kinetic term) to the $H_0'^{KL}$, the ground state of perturbed parent Hamiltonian, H_{KL}' , remains in $\rho_m \neq 0$ sectors, provided that the rough estimate $t_e \lesssim j_m/2$ holds. It ensures that the zero-flux sector is not reachable to avoid getting the ground state of H_0^{KL} . It is worth mentioning that iTEBD algorithm does not guarantee the final wavefunction of H_{KL}' to remain in a sector with finite flux density for arbitrary increasing value of t_e .

The results of our numerical simulation for H_{KL}' with $j_m' = -10j_e$ are presented in Fig. 2-(c), which shows no evidence for a quantum phase transition at $\rho_m \neq 0$. The von-Neumann entropy is $2 \ln 2$, where magnetization is zero, the Schmidt coefficients are degenerate and $\mathcal{O}_{Z_2 \times Z_2} = -1$. All these results indicate the robustness of SPT order as a consequence of self-generated disorder. This effect is also comparable with Ref. 4, in which the *external* random field with dilution distribution stabilizes intrinsic topological order against arbitrarily strong magnetic fields.

Boundary condition for the dual pseudo-spins.—In this section, we study the effect of the flux parity, defined in Eq. (3), on determining the boundary condition (BC) for pseudo-spins $\mu_{r/b}$. Because of the global constraint

$\prod_i \mu_{r,i}^z \mu_{b,i}^z = \mathbb{1}$, $\mu_{r/b}$'s only describe $2L - 1$ independent degrees of freedom. So, applying dual transformation on the original spins of the KL with periodic-BC results a 1-to-2 mapping between $\mu_{r/b}$'s and original spins. One can consider two additional independent ancillary degrees of freedom, in the virtual $(L + 1)$ -th unit cell of the ladder (see Fig. 1). According to our definition for blue and red pseudo-spins, $\mu_{r/b,i}^x = \prod_{j \geq i} Z_{g,j} Z_{r/b,j}$, the x-component of ancillary pseudo-spins are product over an empty set, hence $\mu_{r,L+1}^x = \mu_{b,L+1}^x = 1$. On the other hand, the string operators $\mu_{r,1}^x$ and $\mu_{b,1}^x$ are two special cases that commute with H^{KL} and in terms of the original spins take the form $\mu_{r,1}^x = W_z$, $\mu_{b,1}^x = \Sigma^{IZZ} W_z$. Combination of these properties gives:

$$1 = \mu_{r,L+1}^x = \begin{cases} \mu_{r,1}^x & \text{if } W_z = +1 \\ -\mu_{r,1}^x & \text{if } W_z = -1. \end{cases} \quad (5)$$

In fact, $\mu_{r,1}^x$ and $\mu_{b,1}^x$ are *dynamical variables* that are not independent from each other and determine the BCs on the μ 's. So, according to Eq. (5), the flux parity

$$\Sigma^{IZZ} = \mu_{r,1}^x \mu_{b,1}^x \equiv (-1)^{N_m} = \begin{cases} +1 \\ -1, \end{cases} \quad (6)$$

determines the BC of the red and blue TFI chains in H_{dual}^{KL} and relates them to each other in such a way that for the even parity two chains simultaneously have periodic-BC or antiperiodic-BC, but for the odd parity one chain has periodic-BC while another must have antiperiodic-BC and vice versa. In fact, the mentioned BCs, by doubling the size of the Hilbert space, establishes a 1-to-1 mapping between any energy level of H_{dual}^{KL} and the perturbed KL Hamiltonian.

Time scales of entanglement dynamics.—Here, we investigate the scaling of characteristic times of entanglement dynamics (τ_{int} and τ_{eff}). In Fig. 3, by using exact diagonalization method, we provide the numerical results for available system size, which indicate inverse quadratic scaling of τ_{eff} with t_m , linear scaling with t_e as well as inverse scaling of τ_{int} with t_m .

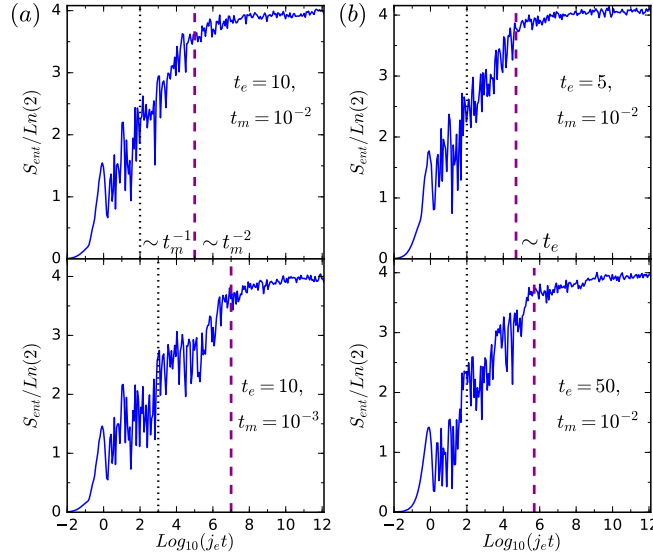


FIG. 3. The temporal growth of half-cut entanglement entropy, averaged over 50 initial product states, for $N = 12$ and $j_m = 10$. The scaling of τ_{int} (black dotted line) and τ_{eff} (purple dashed line) (a) with t_m and (b) with t_e .

Projected Hamiltonian.—As mentioned in the main text, dynamics of the fluxes in our model is governed by the two-body ferromagnetic Ising interaction, $t_m X_i X_j$, between the nearest neighbor spins, that sit on the legs of the ladder. Here, we would like to restrict our study to the effect of flux dynamics on localization or thermalization of finite energy density states, where we discard the creation/annihilation of fluxes which might occurs as a result of $X_i X_j$ terms. Typically, this recombining processes are less likely for the heavy particles in comparison to the light ones, equivalent to $j_m \gg t_e > t_m$. Here, we impose this restriction by projecting the leg-Ising interaction onto the subspace with a fixed total number of flux by $\hat{P}_{N_m} = \sum'_{\{n_i^m\}} \hat{P}_{\{n_i^m\}}$, where $N_m = \sum_i n_i^m$ and $\hat{P}_{\{n_i^m\}}$ is defined in Eq. (1). In this respect, the projected Hamiltonian is given by $\tilde{H}_{KL} = \hat{P}_{N_m} H^{KL} \hat{P}_{N_m}$. Accordingly, the matrix

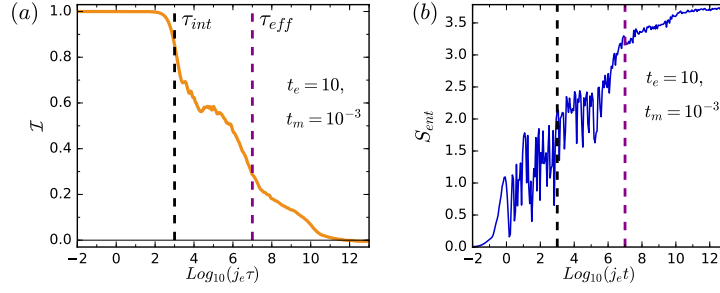


FIG. 4. (a) Relaxation of flux inhomogeneity and (b) Growth of entanglement entropy for subsystem cut at 8-th spin, corresponding to strong effective disorder governed by \tilde{H}_{KL} for $(N, N_m) = (15, 3)$, averaged over 200 random product states.

elements of \tilde{H}_{KL} can only connect different configurations of the flux anyons with fixed N_m . Hence, the total number of fluxes, in addition to the flux parity, will be a constant of motion of \tilde{H}_{KL} , and thus the implementation of this symmetry is more efficient for computational purposes. In this situation, the effective mass of heavy particles living in finite energy levels is inversely controlled by t_m parameter and in every fixed flux sector, j_m is an irrelevant parameter. To check the validity of this approach, in Fig. 4, we compute entanglement dynamics and relaxation of the initial inhomogeneity governed by \tilde{H}_{KL} , which shows the same qualitative behavior in comparison to those governed by H^{KL} , presented in the main text.

Generalization to other SPT phases.—We would like to present a more general picture on the implications of topological order and braiding statistics for the self-localization of anyon excitations in highly excited states. In quantum doubled models such as Levin-Wen models or Kitaev's toric code, an anyon of type a can be transported from site i to site j along the directed path γ connecting the two sites through applying open string operators (Wilson line operators) of type a , W_γ^a . In order to mobilize anyons in the system and let them acquire kinetic energy, we can add $\sum_a \sum_\gamma g_\gamma^a W_\gamma^a$ to the ideal (exactly solvable) Hamiltonian, where g_γ^a is the amplitude of the path γ . Now, imagine two distinct paths γ_1 and γ_2 . The product of the two open string operators along γ_1 and $\bar{\gamma}_2$ (γ_2 with opposite direction), i.e., $W_c \equiv W_{\gamma_1}^a W_{\bar{\gamma}_2}^a = W_{\gamma_1}^a (W_{\gamma_2}^a)^{-1}$, forms a closed string (Wilson loop operator). The resulting loop can take various quantized values depending on the total anyon charge inside path $\gamma_3 \equiv \gamma_1 \bar{\gamma}_2$. Now suppose the path γ encloses total anyon charge equal to b . The Wilson operator W_c measures the braid statistics between anyons a and b and is independent of the path γ_3 (as far as it encompasses the anyon charge b). Therefore, $W_{\gamma_2}^a = W_c W_{\gamma_1}^a$. As a result, the total contribution of the two paths γ_1 and γ_2 is $(g_{\gamma_1}^a + g_{\gamma_2}^a W_c) W_{\gamma_1}^a$. Now, let us assume the two paths γ_1 and γ_2 are related via some symmetry operations, for instance the mirror symmetry with respect to the x axis. In that case, we must choose $|g_{\gamma_1}^a| = |g_{\gamma_2}^a|$ if we want to preserve that symmetry. Since, W_c depends on the total anyon charge trapped inside loop γ_3 and it may take a different value upon the translation of γ_3 , the perturbations can be viewed as disordered anyon hopping terms where the disorder is due to the nontrivial anyon braid statistics as discussed previously.

* langari@sharif.edu

- [1] R. Orús and G. Vidal, *Phys. Rev. B* **78**, 155117 (2008).
- [2] F. Pollmann, A. M. Turner, E. Berg, and M. Oshikawa, *Phys. Rev. B* **81**, 064439 (2010).
- [3] F. Pollmann and A. M. Turner, *Phys. Rev. B* **86**, 125441 (2012).
- [4] D. I. Tsomokos, T. J. Osborne, and C. Castelnovo, *Phys. Rev. B* **83**, 075124 (2011).